LightEndoStereo: A Real-time Lightweight Stereo Matching Method for Endoscopy Images

Yang Ding[1], Can Han[1], Sijia Du[1], Yaqi Wang[2], Dahong Qian[1,*].

Abstract— **Real-time acquisition of accurate depth of scene is essential for automated robotic minimally invasive surgery, and stereo matching with binocular endoscopy can generate such depth. However, existing algorithms struggle with ambiguous tissue boundaries and real-time performance in prevalent high-resolution endoscopic scenes. We propose LightEndoStereo, a lightweight real-time stereo matching method for endoscopic images. We introduce a 3D Mamba Coordinate Attention module to streamline the cost aggregation process by generating position-sensitive attention maps and capturing long-range dependencies across spatial dimensions using the Mamba block. Additionally, we introduce a High-Frequency Disparity Optimization module to refine disparity estimates at tissue boundaries by enhancing high-frequency information in the wavelet domain. Our method is evaluated on the SCARED and SERV-CT datasets, achieving state-of-the-art matching accuracy and a real-time inference speed of 42 FPS. The code is available at https://github.com/Sonne-Ding/LightEndoStereo.**

I. INTRODUCTION

Minimally invasive surgery (MIS) has become a preferred surgical approach due to its reduced invasiveness and faster recovery times [1]. Endoscopy can provide essential visual guidance in MIS. However, endoscopy faces inherent limitations, including a restricted field of view, lack of tactile feedback, and diminished spatial awareness [2], [3], [4]. To address these challenges, computer-assisted intervention (CAI) techniques have been developed to extract spatial depth information from endoscopic images, with depth estimation emerging as a key focus [3].

Endoscopic stereo matching is the method to obtain tissue depth information from binocular images [5], [6]. Specifically, it generates a disparity map that can be converted into a depth map through a simple mapping relationship. Although there have been numerous studies on stereo matching in the domain of natural images, endoscopic stereo matching still faces some challenges due to its unique application scenarios. Tissue boundaries in endoscopic images are blurred due to smooth transitions [7], making accurate depth estimation difficult. Meanwhile, the increasing adoption of high-definition endoscopes adds challenges for stereo matching to maintain computational efficiency and real-time performance. Therefore, developing an efficient, accurate, and robust endoscopic stereo matching method is essential.
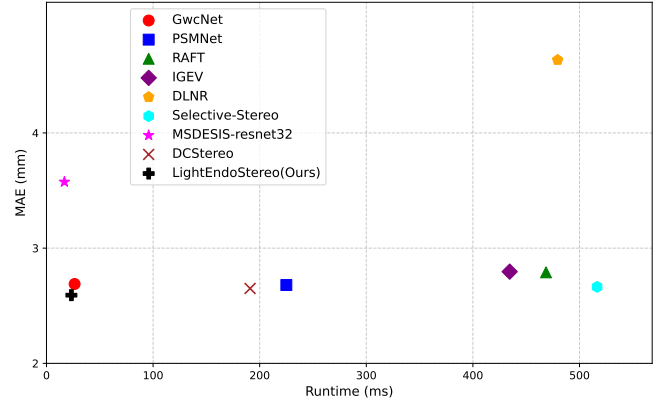
Fig. 1: **Overview of LightEndoStereo.** The figure presents the average MAE and single-frame inference speed of various methods on the SCARED dataset. Our method achieves state-of-the-art (SOTA) matching accuracy while maintaining high inference speed.

Since Jure Zbontar [8] first introduced convolutional neural networks (CNNs) to stereo matching, numerous deep learning-based methods have been proposed in this field. Compared to traditional methods, deep learning approaches, leveraging complex network architectures, adaptive feature extraction, and refined optimization capabilities, have achieved significantly higher matching accuracy [9], [10], [11], [12], [13].Currently, there are two mainstream approaches in stereo matching: those based on 3D convolutions [5], [8], [14], [15], [16], [9], [17], [18] and those based on iterative optimization [19], [20], [21], [22]. Methods based on 3D convolutions can effectively encode essential geometric information for matching. However, they also introduce increased computational complexity [23]. On the other hand, iterative optimization frameworks employ recurrent neural networks (RNNs) to iteratively refine disparity estimation [20], balancing matching accuracy and computational performance by adjusting the number of iterations.When processing high-resolution endoscopic images (e.g., 1024×1280 in the SCARED dataset [24]), these iterative methods often require multiple iterations to achieve satisfactory results. Due to the lack of GPU acceleration, their inference speed lags behind convolution-based methods and fails to meet real-time requirements.

To address the needs of real-time lightweight networks and optimize disparity prediction in tissue regions for endoscopic stereo matching, we propose **LightEndoStereo**, a lightweight real-time stereo matching network. Our approach focuses on three key stages of stereo matching: feature

extraction, cost aggregation, and disparity refinement. In the feature extraction module, we introduce a lightweight feature extraction network based on MobileNetV4 [25]. For cost aggregation, we develop a novel attention module, the **3D Mamba Coordinate Attention (MCA) Module**. This module integrates spatial position information into feature attention and leverages the long-range dependency modeling capability of the Mamba block to achieve effective aggregation across all spatial dimensions. By embedding this module into a simplified 3D UNet aggregation network, we achieve robust aggregation with minimal computational overhead. Our experiments show that the MCA module with 3D UNet outperforms the Stacked Hourglass Network [7], which relies heavily on stacked 3D convolutions. In the disparity refinement stage, we propose the **HFDO (High-Frequency Disparity Optimization)** module to enhance high-frequency details in the disparity map. This module uses the Haar wavelet transform to decompose context features into low- and high-frequency components. It then enhances the high-frequency components and reconstructs the feature map with enhanced high-frequency information via the inverse wavelet transform. The optimized features are projected into the disparity space to refine high-frequency regions.We validate our model on the SCARED dataset [24] and SERV-CT dataset [26], demonstrating its effectiveness and efficiency in real-time endoscopic stereo matching. As shown in Fig. 1, our method achieves the best average MAE of 2.592 mm on the SCARED dataset, with an inference time of 23.38 ms per frame at 1024×1280 resolution.

Our main contributions are summarized as follows:

- We explore stereo matching methods for real-time depth information acquisition via binocular endoscopy in automated minimally invasive surgery, and propose LightEndoStereo, a lightweight real-time stereo matching algorithm that enables accurate disparity estimation, particularly in high-frequency regions such as tissue boundaries and surgical instrument edges.
- To achieve high-quality aggregation of matching costs in 3D space with minimal computational overhead, we propose the 3D Mamba Coordinate Attention (MCA) module. This module incorporates spatial information into channel attention and efficiently captures long-range correlations across the entire 3D space.
- To minimize disparity estimation errors at boundaries, which are particularly evident in endoscopic images, we propose a High-Frequency Disparity Optimization (HFDO) module. This module enhances high-frequency components of context features in the wavelet domain to improve disparity estimation at tissue and instrument boundaries.

II. RELATED WORK

A. Real-time Stereo Matching

For of real-time stereo matching, there are primarily two categories: CNN-based cost aggregation methods and iterative optimization-based methods The use of CNNs in

stereo matching traces back to the nascent stages of deep learning. These methods predominantly utilize CNNs to extract features and construct a cost volume for disparity estimation. CNN-based methods can be divided into 2D and 3D architectures contingent upon the processing of the cost volume. For instance, 2D architectures like DispNet [27] employ 2D convolutions to process the cost volume, thereby achieving real-time performance albeit with relatively lower accuracy. Conversely, 3D architectures, such as [28], [29], [16], utilize 3D convolutions to explicitly encode geometric information, which enhances accuracy but at the expense of high computational complexity.

Iterative optimization-based methods, inspired by iterative refinement techniques in optical flow estimation such as RAFT [30], refine disparity estimates through multiple iterations. RAFT-Stereo [21] is a pioneering work in this domain. RAFT employs a GRU (Gated Recurrent Unit) structure to iteratively optimize the disparity map, achieving a balance between high accuracy and efficiency. Building on this foundation, subsequent methods have further enhanced the iterative optimization process. The CREStereo [22] adopts a hierarchical network design, updating the disparity map through a coarse-to-fine recursive approach to better recover complex image details. The IGEV-Stereo [20] introduces adaptive correlation layers and geometry encoding volumes to improve the robustness and accuracy of the models. Similarly, DLNR [19] employs an LSTM (Long-Short-Term Memory) structure to specifically optimize disparity estimates in high-frequency regions, thereby further bolstering the overall performance of the models.

B. High-Frequency Optimization in Stereo Matching

Several works have focused on optimizing stereo matching for high-frequency components [19], [31], [32].The DLNR [19] highlights that the coupling between the update matrix and the hidden state transfer in the GRU module used by RAFT can lead to inaccuracies in high-frequency detail prediction. To address this, DLNR introduced an LSTM (Long-Short-Term Memory) structure to replace the GRU, thereby achieving better high-frequency disparity prediction performance. The Selective-Stereo [31] highlighted that GRUs with fixed receptive fields struggle to capture both high-frequency information in edges and low-frequency information in smooth regions simultaneously. To overcome this limitation, Selective-Stereo proposed the Selective Recurrent Unit (SRU), which incorporates multi-scale receptive fields into the GRU design. This approach enables the model to optimize across multiple frequency bands, improving the overall accuracy of disparity prediction.

III. METHOD

In this section, we present the methodology of LightEndoStereo, a lightweight stereo matching algorithm designed for high-precision disparity estimation while maintaining efficient computational performance. We integrate a lightweight feature extraction network, an MCA module for optimized cost aggregation, and an HFDO module to refine
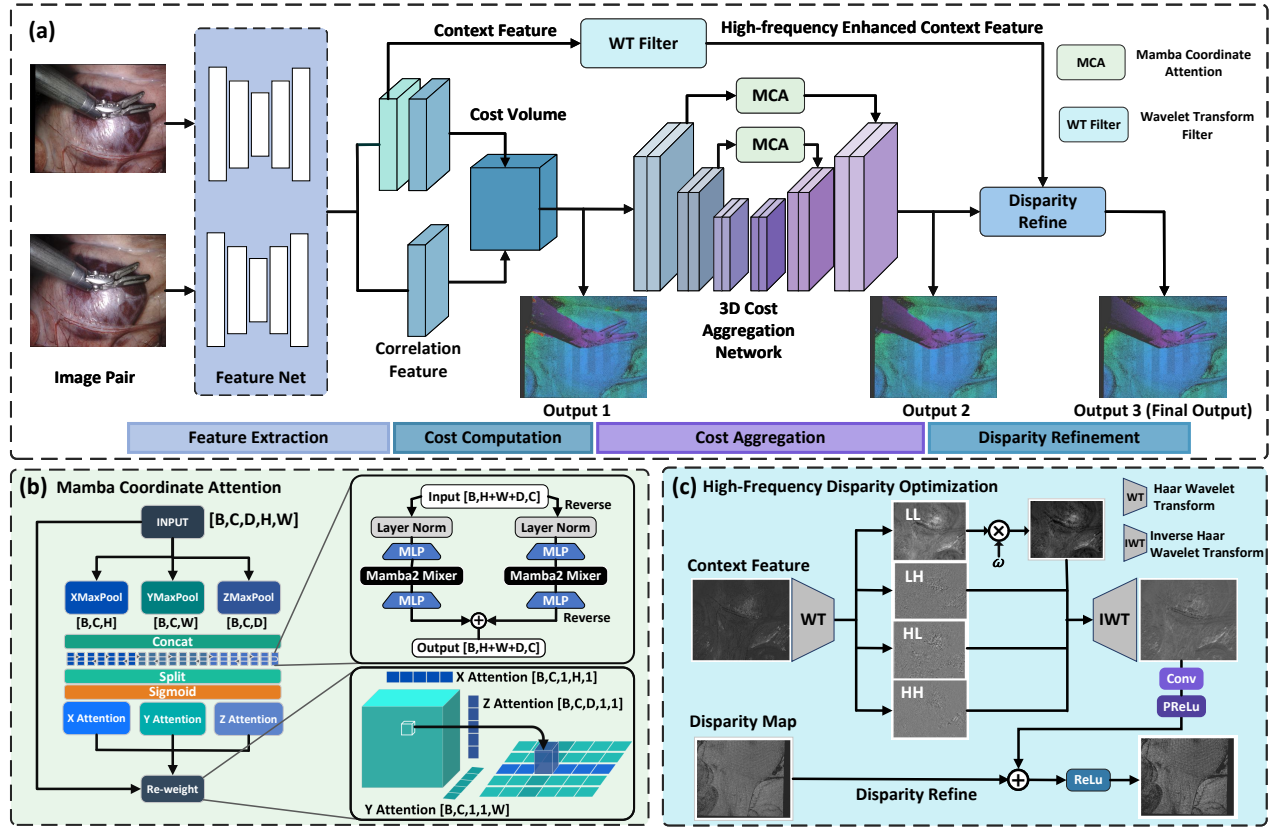
Fig. 2: **(a)** Architecture of LightEndoStereo. The Feature Net is a UNet-like structure with an encoder branch based on MobileNetV4. The group-wise correlation cost volume is utilized. **(b)** Mamba Coordinate Attention module. Attention is extracted separately across the H, W, and D dimensions, concatenated along the channel dimension, and then passed through a Bi-Mamba2 layer. Bi-Mamba2 layer extracts dependencies between features in both forward and backward directions across all spatial dimensions $(H + W + D)$. The resulting position-sensitive attention maps are used to re-weight the feature map. **(c)** Wavelet Transform Refine module. The context feature map is decomposed into low-frequency (LL) and high-frequency (LH, HL, HH) components. The LL components are attenuated by a parameter w.

disparities in high-frequency regions. The overall architecture is shown in Fig. 2.

A. Feature Extraction

Multi-scale information is essential for stereo matching. Shallow features capture rich texture and geometric details, while deep features provide important abstract semantic information. As so, we propose a lightweight multi-scale feature extraction network based on the U-Net architecture. The encoder branch utilizes MobileNetV4, an efficient lightweight neural network optimized for mobile devices. In the decoder stage, we employ 2D convolutions and skip connections between adjacent scales to progressively restore multi-scale information.

Given a stereo pair $I_l, I_r \in \mathbb{R}^{3 \times H \times W}$, we utilize the MobileNetV4 structure [25] as the downsampling branch of the U-Net multi-scale feature extraction framework. In the upsampling branch, features at scales of 1/16, 1/8, and 1/4 are fused, resulting in the final output features at a 1/4 scale of the original image, $F_l, F_r \in \mathbb{R}^{C \times H/4 \times W/4}$. The feature F_l extracted from the encoder branch serves as the context

feature for subsequent disparity optimization.

B. Cost Volume Computation

We employ a Group-wise Correlation cost volume [16] to compute the matching cost between the extracted paired features. For the feature maps F_l and F_r, we divide the channels into g_n groups, where $g_n = 16$ in this work. Within each group, the feature vectors from the left and right images are correlated via the inner product. The cost volume is then constructed by concatenating the correlation results across groups. The cost volume is defined as:

$$CV(g, d, x, y) = \frac{1}{C/g_n} \langle F_l^g(x, y), F_r^g(x - d, y) \rangle, \quad (1)$$

where CV denotes the cost volume, F_*^g represents the feature vectors within group g ($g \in [0, g_n - 1]$), and $\langle \cdot, \cdot \rangle$ denotes the inner product.

C. 3D Mamba Coordinate Attention Guided Cost Aggregation

We propose a novel 3D Mamba Coordinate Attention module. This module extends the coordinate attention framework

by embedding positional information into channel attention. Moreover, to capture long-range interactions among channel features across the disparity, width, and height dimensions, we introduce a bidirectional Mamba2 block.

Specifically, for the cost volume $CV \in \mathbb{R}^{g_n \times D \times H \times W}$, we treat the disparity dimension D as an additional spatial dimension. We employ three pooling kernels (H,W), (D,H), and (D,W) to perform channel encoding along the horizontal, vertical, and disparity directions, respectively. For a given 3D feature $\mathscr{F} \in \mathbb{R}^{C \times X \times Y \times Z}$ (where Z dimension corresponds to the disparity D in this work), the channel-wise attention extraction for the c-th channel along the three directions is formulated as:

$$
\begin{aligned}
\mathscr{Z}_c^x(x) &= \frac{1}{Y \cdot Z} \max_{y,z} \mathscr{F}(c,x,y,z), \\
\mathscr{Z}_c^y(y) &= \frac{1}{X \cdot Z} \max_{x,z} \mathscr{F}(c,x,y,z), \\
\mathscr{Z}_c^z(z) &= \frac{1}{X \cdot Y} \max_{x,y} \mathscr{F}(c,x,y,z).
\end{aligned}
\tag{2}
$$

Subsequently, we introduce non-linearity via a sigmoid function and employ the Mamba2 module to capture long-range dependencies across all spatial dimensions. The refined spatial attention is computed as:

$$
\begin{aligned}
A_{\text{refined}} &= \text{Mamba2}\left(\text{concat}\left([\delta(\mathscr{Z}^x), \delta(\mathscr{Z}^y), \delta(\mathscr{Z}^z)]\right)\right), \\
A_x, A_y, A_z &= \text{split}(A_{\text{refined}}),
\end{aligned}
\tag{3}
$$

where $\delta(\cdot)$ denotes the sigmoid function. Finally, the refined attention maps A_x, A_y, and A_z are applied to the original feature map $\mathscr{F}$ to obtain the optimized feature map:

$$
\mathscr{F}_{\text{refined}} = \mathscr{F} \odot A_x \odot A_y \odot A_z,
\tag{4}
$$

where $\odot$ denotes broadcast A_* and then performs element-wise multiplication. The proposed 3D MCA module is embedded into a light 3 scale 3D UNet cost aggregation network to enhance the model's ability to capture long-range dependencies across the entire spatial domain. We refer to this aggregation network as 3D UNet-MCA in the following text.

D. Disparity Computation

To achieve differentiable disparity computation and generate sub-pixel disparity estimates with higher precision, we utilize the soft argmax operation to calculate the disparity [28]. Specifically, the matching cost volume CV is first processed by reducing its feature dimension to 1. Subsequently, the spatial scale is restored through bilinear interpolation, resulting in the final cost volume $CV \in \mathbb{R}^{D \times H \times W}$.

The operations are formulated as follows:

$$
CV = \text{Interpolate}(\text{Conv}(CV)),
\tag{5}
$$

where Conv denotes the convolution operation that compresses the feature dimension, and Interpolate represents the bilinear interpolation for spatial scale recovery.

The disparity at each pixel location (h,w) is then computed using the soft argmax operation:

$$
d(h,w) = \sum_{i=0}^{D-1} i \times \sigma(CV(i,h,w)),
\tag{6}
$$

where σ is the softmax function.

E. High Frequency Disparity Optimization

In endoscopic images, depth variations are relatively gradual in most regions. This characteristic poses challenges for the model in predicting depth in high-frequency regions, while the boundaries and blood vessels are not prominent in the images. To enhance the optimization of high-frequency regions in the disparity optimization process, while avoiding introducing noise to the well-predicted low-frequency regions, we employ a wavelet module. This module decomposes the context feature F_s obtained from F_l into low-frequency components(LL) and high-frequency components in horizontal(LH), vertical(HL), and diagonal directions(HH). The low-frequency components are then attenuated by a scale ω, and the inverse wavelet transform is applied to obtain the refined context feature. The refined context feature specifically targets the optimization of high-frequency detail regions in the disparity map.

The context features are derived as follows:

$$
F_s = \text{ReLU}(\text{Linear}(F_l)),
\tag{7}
$$

where Conv denotes a 2D 3×3 convolution. The 2D Haar wavelet convolution kernels used are [33]:

$$
\begin{aligned}
h_{LL} &= \frac{1}{2}\begin{bmatrix} 1 & 1 \\ 1 & 1 \end{bmatrix}, \quad h_{LH} = \frac{1}{2}\begin{bmatrix} 1 & -1 \\ 1 & -1 \end{bmatrix}, \\
h_{HL} &= \frac{1}{2}\begin{bmatrix} 1 & 1 \\ -1 & -1 \end{bmatrix}, h_{HH} = \frac{1}{2}\begin{bmatrix} 1 & -1 \\ -1 & 1 \end{bmatrix}.
\end{aligned}
\tag{8}
$$

The decomposition of the feature map F_s is performed as follows:

$$
\begin{aligned}
F_s^{ll} &= \omega \cdot (h_{LL} * F_s), \quad F_s^{lh} = h_{LH} * F_s, \\
F_s^{hl} &= h_{HL} * F_s, \quad F_s^{hh} = h_{HH} * F_s,
\end{aligned}
\tag{9}
$$

where ω is the attenuation factor for the low-frequency components. The feature map is then reconstructed using the inverse wavelet transform:

$$
F_s^{\text{filtered}} = \text{IWT}(F_s^{ll}, F_s^{lh}, F_s^{hl}, F_s^{hh}).
\tag{10}
$$

The filtered semantic features F_s^{filtered} are projected into the disparity space through a Conv layer with a PReLU activation function to generate the optimized disparity map. PReLUis an improved version of the ReLU activation function. It addresses the issue of ReLU's zero output for negative inputs by introducing a learnable parameter α (Eq. 12). Finally, the optimized disparity map is processed using a ReLU activation function to ensure that the disparity values are non-negative:

$$
D_{refined} = \text{ReLU}(D + \text{PReLU}(\text{Conv}(F_s^{filtered}))),
\tag{11}
$$

$$
\text{PReLU}(x) = \begin{cases} x & \text{if } x \geq 0, \\ \alpha x & \text{if } x < 0. \end{cases}
\tag{12}
$$

F. Loss Function

We utilize the *smoothL*$_1$ loss(Eq. 13) to quantify the discrepancy between the predicted disparity map and the ground-truth disparity map. Specifically, we compute the loss at three critical stages of the disparity estimation pipeline: prior to cost aggregation (d_f), before disparity optimization (d_{cg}), and at the final output stage (d_{dr}).:

$$L_{smooth}(x) = \begin{cases} 0.5x^2 & \text{if } |x| < 1, \\ |x| - 0.5 & \text{otherwise.} \end{cases} \quad (13)$$

The total loss is formulated as:

$$\text{Loss} = w_1 \cdot \|d_f - d_{gt}\|_1 + w_2 \cdot \|d_{cg} - d_{gt}\|_1 + \\ w_3 \cdot \|d_{dr} - d_{gt}\|_1, \quad (14)$$

where w_1, w_2, and w_3 are the weights assigned to the losses at each respective stage(we set $w_1 = w_2 = w_3 = 1/3$).

IV. EXPERIMENTS

A. Datasets

We trained our algorithm on the SCARED dataset and tested it on both the SCARED and SERV-CT datasets.

1) SCARED Dataset [24]: The SCARED dataset [24] is a public laparoscopy dataset from the MICCAI 2019 Endovis Challenge, captured using the da Vinci Xi surgical robot. It consists of porcine peritoneal images with a resolution of 1024×1280. The dataset includes 7 training subsets and 2 test subsets. Due to significant calibration errors in datasets 4 and 5, we discarded these subsets and trained our model using the remaining training data (14,714 image pairs). The dataset 8 and 9 are testing data. We adopt the official evaluation metric: Mean Absolute Error (MAE) in mm of the depth map.

2) SERV-CT Dataset [26]: The SERV-CT dataset [26] contains 16 pairs of porcine peritoneal stereo images with a resolution of 720×576. We use all 16 pairs for testing. We evaluate performance using the Mean Absolute Error (MAE) in pixels, the percentage of pixels with a disparity error greater than n pixels (Bad-n), and the percentage of pixels with an error greater than 3 pixels and greater than 5% of the ground-truth value (D1).

B. Implementation details

We adopted a MobileNetV4, pre-trained on ImageNet, as the decoder part branch of feature network. The model was implemented using the PyTorch framework. For optimization, we utilized the Adam optimizer with $\beta_1 = 0.9$ and $\beta_2 = 0.999$. The learning rate for the feature network is 1×10^{-4} and 1×10^{-3} for the other parts. During training, we set the random seed to 6. For data augmentation, we applied random cropping to resize the training images to 256×512. The model was trained for 100 epochs on the SCARED dataset. For evaluation, we tested the model on datasets 8 and 9 of SCARED, as well as the SERV-CT dataset. All experiments were conducted on an Ubuntu 22.04 system with 4 Nvidia RTX 2080Ti GPUs.

TABLE I: MAE (unit: mm) for the SCARED Test Set. Each test set comprises 5 keyframes (kf1–kf5). Lower values indicate better performance. Methods marked with (*) reference results from other papers. Bold font indicates the optimal results.

Method	Dataset 8					Dataset 9					Avg.
	kf1	kf2	kf3	kf4	kf5	kf1	kf2	kf3	kf4	kf5	
GwcNet [16]	9.076	2.926	1.433	**1.7**	1.203	3.868	1.138	2.934	1.997	0.6135	2.689
PSMNet* [29]	8.96	2.77	**1.43**	1.83	1.42	3.99	1.08	2.82	1.95	0.56	2.68
RAFT [21]	7.921	2.362	1.721	2.167	1.88	4.363	1.087	2.872	1.983	1.549	2.79
IGEV [20]	7.955	2.393	1.697	2.265	1.938	3.893	1.174	2.895	2.504	1.25	2.796
DLNR [19]	7.848	2.529	2.654	3.209	3.418	5.374	1.913	4.324	4.82	10.25	4.634
Selective-Stereo [31]	7.537	2.409	1.668	2.31	2.264	**3.86**	**0.958**	2.838	1.775	1.018	2.664
MSDESIS-resnet32 [7]	10.14	3.467	3.306	3.889	2.099	5.428	1.636	3.378	**1.768**	0.6375	3.575
MSDESIS-light [7]	11.45	15.91	7.727	10.67	9.849	98.39	130.8	66.57	101.8	203.4	65.67
DCStereo* [34]	8.38	2.77	1.54	1.82	1.19	3.99	1.09	**2.64**	2.09	1.04	2.65
LightEndoStereo(Ours)	7.62	**2.316**	1.669	2.281	**1.025**	4.428	1.167	2.809	2.125	**0.4793**	**2.592**

TABLE II: Results of comparison experiments on the SERV-CT dataset.Methods marked with (*) reference results from other papers. Bold font indicates the optimal results.

Model	MAE(pixel)↓	D1↓	Bad1↓	Bad2↓	Bad3↓
GwcNet [16]	5.813	33.92%	79.37%	56.32%	40.93%
PSMNet* [29]	6.355	-	70.88%	49.80%	33.87%
RAFT [21]	21.500	87.50%	95.80%	91.80%	88.50%
IGEV [20]	32.895	92.91%	98.28%	96.53%	94.76%
DLNR [19]	22.030	88.97%	96.21%	92.61%	89.13%
Selective-Stereo [31]	24.103	86.36%	95.68%	91.33%	87.01%
MSDESIS-resnet32 [7]	5.742	28.26%	78.81%	55.44%	37.79%
MSDESIS-light [7]	7.065	41.35%	81.09%	63.17%	49.22%
LightEndoStereo(Ours)	**2.367**	**14.34%**	**58.59%**	**31.52%**	**18.49%**

C. Evaluations on SCARED and SERV-CT

We evaluated our algorithm against several methods for natural image stereo matching and two algorithms for endoscopic data. Specifically, GwcNet [16], PSM-Net [29], RAFT [35], IGEV [20], DLNR [19], and Selective-Stereo [31] are methods designed for natural images, with DLNR and Selective-Stereo focusing on optimizing high-frequency details in disparity maps. For these natural image methods, except for PSMNet, we retrained them on the SCARED dataset. For PSMNet, we directly cited the results from [34], [3]. MSDESIS [7] and DCStereo [34] are algorithms tailored for endoscopic images. DCStereo's evaluation methodology on SCARED aligns with ours, so we directly cited their results. However, since DCStereo was not tested on the SERV-CT dataset and its code is not publicly available, we omitted their results on SERV-CT. MSDESIS was trained on the SCARED dataset, and we directly loaded their pre-trained weights. Given that our maximum disparity is set to 192, whereas MSDESIS uses a maximum disparity of 320, the results we reproduced differ slightly from those reported in their paper. The evaluation results on SCARED are shown in Table I, and the results on SERV-CT are shown in Table II. LightEndoStereo achieved SOTA performance on both datasets and demonstrated excellent generalization on SERV-CT.

D. Runtime Evaluation

To evaluate the runtime performance of our model, we conducted tests using a single Nvidia RTX 2080Ti GPU, paired with an Intel(R) Xeon(R) Gold 6130T CPU @ 2.10GHz. We sampled 100 images (1280×1024) from dataset 8 of the SCARED dataset for testing and used the
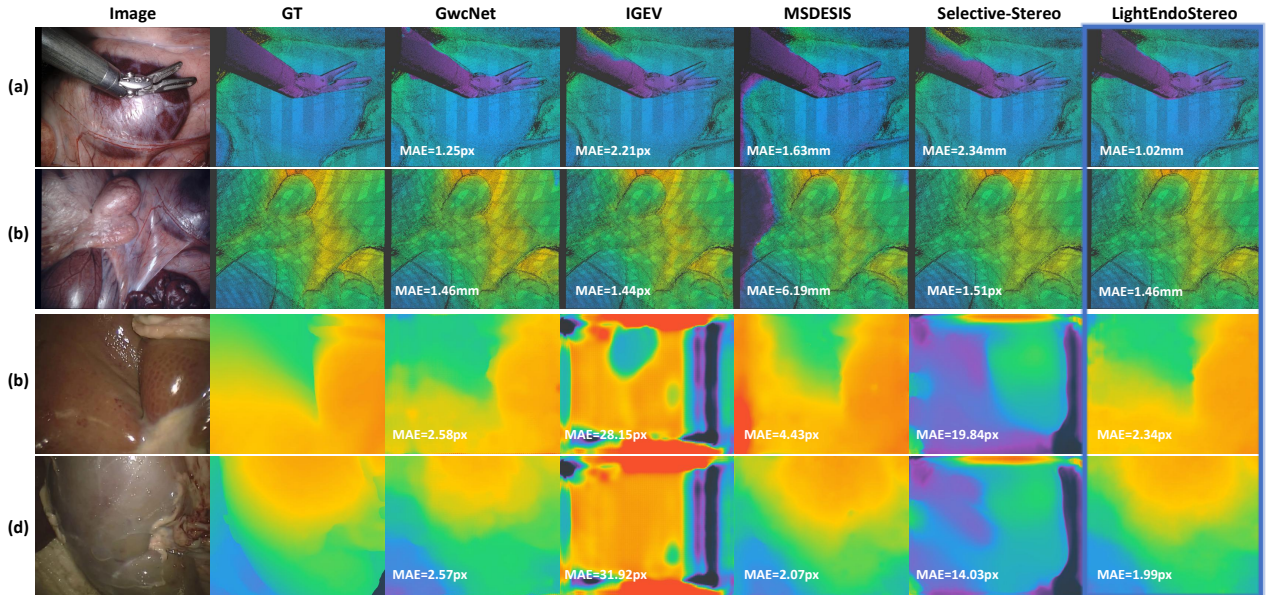
Fig. 3: Visualization of disparity estimation on SCARED and SERV-CT datasets. (a) and (b) are from SCARED, while (c) and (d) are from SERV-CT. When overall depth variation is minimal, as in (b), most models perform similarly. However, in scenes with significant depth transitions—indicating high-frequency components, such as between surgical instruments and tissues in (a)—LightEndoStereo provides more accurate depth estimates at boundary regions. Figures (c) and (d) show that LightEndoStereo also performs well on SERV-CT.

TABLE III: Quantitative results of model computational performance. Note that only methods with an average MAE < 3mm on the SCARED dataset are included. Methods marked with (*) reference results from other papers. Bold font indicates the optimal results.

Model	Params(M)	FLOPs(T)	Runtimes(ms)
GwcNet [16]	6.43	2.466	26.4
PSMNet* [29]	3.672	-	225
RAFT [21]	11.11	3.757	468.6
IGEV [20]	12.5	3.288	434.5
Selective-Stereo [31]	13.141	4.062	516.52
DCStereo* [34]	**3.404**	-	191
LightEndoStereo(Ours)	11.094	**0.846**	**23.38**

average inference time as the evaluation metric. The results are shown in Table III. Although the MSDESIS-Light model has the smallest footprint, its matching accuracy is poor. In contrast, LightEndoStereo achieved a real-time matching speed of 23.38 ms per frame.

TABLE IV: Ablation Study Results. We use the average MAE on the SCARED dataset as the accuracy evaluation metric. When ablating the 3D UNet-MCA, we employ the widely-used 3D Hourglass aggregation network.

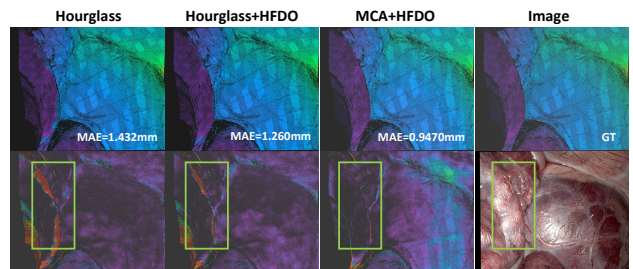| 3D UNet-MCA	HFDO	MAE(mm)	Runtime(ms)	Params(M)	FLOPs(T)
		2.718	25.412ms	13.0479	1.7552
	✓	2.645	25.972ms	13.0773	1.7579
✓		2.621	22.655ms	11.0649	0.8435
✓	✓	2.592	23.386ms	11.0943	0.8461

Fig. 4: Visualization of disparity optimization in high-frequency regions. The top row shows the depth maps, while the bottom row displays the corresponding error maps.

E. Ablation Study

We conducted detailed ablation studies on the proposed 3D MCA and HFDO modules (see Table IV). When ablating the 3D UNet-MCA aggregation network, we employ the widely-used 3D Hourglass aggregation network [16]. The 3D Hourglass aggregation network is a stacked symmetric multi-scale network that features a large number of parameters and high computational complexity. As shown in Table III, the 3D UNet-MCA not only reduces the number of parameters and computational complexity but also enhances disparity estimation accuracy. As Figure 4 illustrates, the HFDO module significantly reduces matching errors at tissue boundaries, leading to notable improvements in both the Stacked 3D Hourglass and 3D UNet-MCA configurations.

V. CONCLUSIONS AND LIMITATIONS

We introduce LightEndoStereo, a novel lightweight real-time stereo matching algorithm tailored for endoscopic images. Our approach integrates a coordinate attention mechanism and the Mamba block to achieve efficient cost aggregation via a lightweight 3D UNet. Moreover, by enhancing high-frequency features in the wavelet domain, we optimize disparity estimation, effectively mitigating large matching errors at tissue boundaries—a common challenge in endoscopic stereo matching. During validation, LightEndoStereo exhibited strong generalization on the SERV-CT dataset, a potential that warrants further exploration. Acknowledging the significance of generalizable stereo matching algorithms, we intend to delve deeper into this area in our future research.

REFERENCES

[1] E. P. Westebring-van der Putten, R. H. Goossens, J. J. Jakimowicz, and J. Dankelman, "Haptics in minimally invasive surgery–a review," *Minimally Invasive Therapy & Allied Technologies*, vol. 17, no. 1, pp. 3–16, 2008.

[2] X. Cheng, Y. Zhong, M. Harandi, T. Drummond, Z. Wang, and Z. Ge, "Deep laparoscopic stereo matching with transformers," in *International Conference on Medical Image Computing and Computer-Assisted Intervention*. Springer, 2022, pp. 464–474.

[3] R. Wu, P. Liang, Y. Liu, Y. Huang, W. Li, and Q. Chang, "Laparoscopic stereo matching using 3-dimensional fourier transform with full multi-scale features," *Engineering Applications of Artificial Intelligence*, vol. 139, p. 109654, 2025.

[4] D. Scharstein and R. Szeliski, "A taxonomy and evaluation of dense two-frame stereo correspondence algorithms," *International journal of computer vision*, vol. 47, pp. 7–42, 2002.

[5] Y. Zhang, M. Poggi, and S. Mattoccia, "Temporalstereo: Efficient spatial-temporal stereo matching network," in *2023 IEEE/RSJ International Conference on Intelligent Robots and Systems (IROS)*. IEEE, 2023, pp. 9528–9535.

[6] J. Cartucho, S. Tukra, Y. Li, D. S. Elson, and S. Giannarou, "Visionblender: a tool to efficiently generate computer vision datasets for robotic surgery," *Computer Methods in Biomechanics and Biomedical Engineering: Imaging & Visualization*, vol. 9, no. 4, pp. 331–338, 2021.

[7] D. Psychogyios, E. Mazomenos, F. Vasconcelos, and D. Stoyanov, "Msdesis: Multitask stereo disparity estimation and surgical instrument segmentation," *IEEE transactions on medical imaging*, vol. 41, no. 11, pp. 3218–3230, 2022.

[8] J. Zbontar and Y. LeCun, "Computing the stereo matching cost with a convolutional neural network," in *Proceedings of the IEEE conference on computer vision and pattern recognition*, 2015, pp. 1592–1599.

[9] S. Duggal, S. Wang, W.-C. Ma, R. Hu, and R. Urtasun, "Deeppruner: Learning efficient stereo matching via differentiable patchmatch," in *Proceedings of the IEEE/CVF international conference on computer vision*, 2019, pp. 4384–4393.

[10] Y. Zhang, S. Khamis, C. Rhemann, J. Valentin, A. Kowdle, V. Tankovich, M. Schoenberg, S. Izadi, T. Funkhouser, and S. Fanello, "Activestereonet: End-to-end self-supervised learning for active stereo systems," in *Proceedings of the european conference on computer vision (ECCV)*, 2018, pp. 784–801.

[11] I. K. Park *et al.*, "Deep self-guided cost aggregation for stereo matching," *Pattern Recognition Letters*, vol. 112, pp. 168–175, 2018.

[12] Z. Huang, J. Gu, J. Li, and X. Yu, "A stereo matching algorithm based on the improved psmnet," *Plos one*, vol. 16, no. 8, p. e0251657, 2021.

[13] M. Shen, Y. Gu, N. Liu, and G.-Z. Yang, "Context-aware depth and pose estimation for bronchoscopic navigation," *IEEE Robotics and Automation Letters*, vol. 4, no. 2, pp. 732–739, 2019.

[14] A. Badki, A. Troccoli, K. Kim, J. Kautz, P. Sen, and O. Gallo, "Bi3d: Stereo depth estimation via binary classifications," in *Proceedings of the IEEE/CVF Conference on Computer Vision and Pattern Recognition*, 2020, pp. 1600–1608.

[15] Z. Shen, Y. Dai, X. Song, Z. Rao, D. Zhou, and L. Zhang, "Pcw-net: Pyramid combination and warping cost volume for stereo matching," in *European conference on computer vision*. Springer, 2022, pp. 280–297.

[16] X. Guo, K. Yang, W. Yang, X. Wang, and H. Li, "Group-wise correlation stereo network," in *Proceedings of the IEEE/CVF conference on computer vision and pattern recognition*, 2019, pp. 3273–3282.

[17] J. Žbontar and Y. LeCun, "Stereo matching by training a convolutional neural network to compare image patches," *Journal of Machine Learning Research*, vol. 17, no. 65, pp. 1–32, 2016.

[18] H. Xu and J. Zhang, "Aanet: Adaptive aggregation network for efficient stereo matching," in *Proceedings of the IEEE/CVF conference on computer vision and pattern recognition*, 2020, pp. 1959–1968.

[19] H. Zhao, H. Zhou, Y. Zhang, J. Chen, Y. Yang, and Y. Zhao, "High-frequency stereo matching network," in *Proceedings of the IEEE/CVF conference on computer vision and pattern recognition*, 2023, pp. 1327–1336.

[20] G. Xu, X. Wang, X. Ding, and X. Yang, "Iterative geometry encoding volume for stereo matching," in *Proceedings of the IEEE/CVF conference on computer vision and pattern recognition*, 2023, pp. 21919–21928.

[21] L. Lipson, Z. Teed, and J. Deng, "Raft-stereo: Multilevel recurrent field transforms for stereo matching," in *2021 International Conference on 3D Vision (3DV)*. IEEE, 2021, pp. 218–227.

[22] J. Li, P. Wang, P. Xiong, T. Cai, Z. Yan, L. Yang, J. Liu, H. Fan, and S. Liu, "Practical stereo matching via cascaded recurrent network with adaptive correlation," in *Proceedings of the IEEE/CVF conference on computer vision and pattern recognition*, 2022, pp. 16263–16272.

[23] H. Xu and J. Zhang, "Aanet: Adaptive aggregation network for efficient stereo matching," in *Proceedings of the IEEE/CVF conference on computer vision and pattern recognition*, 2020, pp. 1959–1968.

[24] M. Allan, J. Mcleod, C. Wang, J. C. Rosenthal, Z. Hu, N. Gard, P. Eisert, K. X. Fu, T. Zeffiro, W. Xia, *et al.*, "Stereo correspondence and reconstruction of endoscopic data challenge," *arXiv preprint arXiv:2101.01133*, 2021.

[25] D. Qin, C. Leichner, M. Delakis, M. Fornoni, S. Luo, F. Yang, W. Wang, C. Banbury, C. Ye, B. Akin, *et al.*, "Mobilenetv4: universal models for the mobile ecosystem," in *European Conference on Computer Vision*. Springer, 2024, pp. 78–96.

[26] P. Eddie"Edwards, D. Psychogyios, S. Speidel, L. Maier-Hein, and D. Stoyanov, "Serv-ct: A disparity dataset from ct for validation of endoscopic 3d reconstruction," *arXiv e-prints*, pp. arXiv–2012, 2020.

[27] N. Mayer, E. Ilg, P. Hausser, P. Fischer, D. Cremers, A. Dosovitskiy, and T. Brox, "A large dataset to train convolutional networks for disparity, optical flow, and scene flow estimation," in *Proceedings of the IEEE conference on computer vision and pattern recognition*, 2016, pp. 4040–4048.

[28] A. Kendall, H. Martirosyan, S. Dasgupta, P. Henry, R. Kennedy, A. Bachrach, and A. Bry, "End-to-end learning of geometry and context for deep stereo regression," in *Proceedings of the IEEE international conference on computer vision*, 2017, pp. 66–75.

[29] J.-R. Chang and Y.-S. Chen, "Pyramid stereo matching network," in *Proceedings of the IEEE conference on computer vision and pattern recognition*, 2018, pp. 5410–5418.

[30] Z. Teed and J. Deng, "Raft: Recurrent all-pairs field transforms for optical flow," in *Computer Vision–ECCV 2020: 16th European Conference, Glasgow, UK, August 23–28, 2020, Proceedings, Part II 16*. Springer, 2020, pp. 402–419.

[31] X. Wang, G. Xu, H. Jia, and X. Yang, "Selective-stereo: Adaptive frequency information selection for stereo matching," in *Proceedings of the IEEE/CVF Conference on Computer Vision and Pattern Recognition*, 2024, pp. 19701–19710.

[32] Y. Liu, J. Ren, J. Zhang, J. Liu, and M. Lin, "Visually imbalanced stereo matching," in *Proceedings of the IEEE/CVF Conference on Computer Vision and Pattern Recognition*, 2020, pp. 2029–2038.

[33] S. E. Finder, R. Amoyal, E. Treister, and O. Freifeld, "Wavelet convolutions for large receptive fields," in *European Conference on Computer Vision*. Springer, 2024, pp. 363–380.

[34] Z. Jin, C. Hu, Z. Fu, C. Zhang, P. Wang, H. Zhang, and X. Ye, "Stereo matching of binocular laparoscopic images with improved densely connected neural architecture search," *International Journal of Computer Assisted Radiology and Surgery*, vol. 19, no. 4, pp. 677–686, 2024.

[35] L. Lipson, Z. Teed, and J. Deng, "Raft-stereo: Multilevel recurrent field

transforms for stereo matching," in *2021 International Conference on 3D Vision (3DV)*.   IEEE, 2021, pp. 218–227.